A Parameterization for the Triggering of Landscape-Generated Moist Convection. Part II: Zero-Order and First-Order Closure

BARRY H. LYNN*

Columbia University Center for Climate Systems Research, New York, New York

WEI-KUO TAO

Mesoscale Atmospheric Processes Branch, NASA Goddard Space Flight Center, Greenbelt, Maryland

(Manuscript received 4 January 1999, in final form 5 July 2000)

ABSTRACT

To improve the triggering of clouds over landscape heterogeneity, it is suggested that the forcing by mesoscale circulations generated by landscape patches be included. For this purpose, it is suggested that a relatively simple zero-order closure be used to obtain a triggering parcel's mesoscale perturbation vertical velocity, potential temperature, and specific humidity. In combination with a turbulent fluctuation averaged over a parcel area, one can obtain a parcel's (total) velocity, temperature, and moisture. The authors used similarity theory to parameterize the mesoscale perturbations, using a dataset generated by a three-dimensional, high-resolution cumulus ensemble model with west-to-east land surface patches.

Alternatively, the authors used one-dimensional budget equations that contain mesoscale and turbulent fluctuations (and source terms) to obtain the vertical profile of potential temperature and specific humidity within a triggering parcel. Here, it is suggested that first-order closure be used; these equations with first-order closure should provide more realistic profiles of temperature and moisture within a triggering parcel than with the zero-order scheme above. This is especially the case when moist (cloud) processes occur. An analysis of the model-produced dataset indicated that parameterizations for two terms needed to be developed to close the budget equations: the vertical flux of the mesoscale temperature and moisture. Similarity theory is used to parameterize these fluxes.

1. Introduction

Pielke et al. (1991), Avissar and Chen (1993), and Lynn et al. (1995b, 1998, 2001) have shown that landscape-generated mesoscale circulations (LGMCs) can strongly effect the profile of the vertical velocity, temperature, and moisture within the planetary boundary layer (PBL). Chen and Avissar (1994), Hong et al. (1995), and Lynn et al. (1998) used numerical models to show that landscape-generated mesoscale circulations can trigger both shallow and deep moist convection. Observational results suggest that mesoscale circulations generated by landscape patches can affect the formation of shallow clouds (Rabin et al. 1990: Cutrim et al. 1995). Pielke et al. (1997) has shown that gradients in heat fluxes induced by vegetation change can affect the development of mesoscale convective complexes. For this reason, the development of triggering functions for LGMCs has been the subject of recent work.

Triggering functions are used to determine if moist convection should be initiated by the cumulus parameterization scheme in a mesoscale or regional-scale atmospheric model. Rogers and Fritsch (1996) and Hong and Pan (1998) include in their triggering function the contribution from both mesoscale and turbulent perturbations. This combination is then used to diagnose possible parcels, which are then tested in triggering functions for their capability to initiate moist convection.

Not all triggering functions use the same variables. For example, Rogers and Fritsch (1996) developed a diagnostic relationship [see Eq. (1), in Part I (Lynn et al. 2001)] for the mesoscale contribution to the subgrid-scale vertical velocity within a large-scale model (or even regional-scale mesoscale model), while Hong and Pan (1998) formulated a diagnostic relationship for a subgrid-scale mesoscale temperature perturbation. Thus, Rogers and Fritsch (1996) compare in their trigger function the energy of a parcel with the inhibition energy, while Hong and Pan (1998) compare the bouyancy of

* Current affiliation: Department of Atmospheric Sciences, The Hebrew University of Jerusalem, Jerusalem, Israel.

Corresponding author address: Dr. Barry Lynn, Department of Atmospheric Sciences, The Hebrew University of Jerusalem, Jerusalem, 91904, Israel.
E-mail: barry@dina.es.huji.ac.il

© 2001 American Meteorological Society

a parcel to its environment. Note, each uses simple, empirical relationships that relate the size of the mesocale perturbation to the average size of patches within the domain of the large-scale model. These relationships exclude the effect of gradients in soil moisture, background wind, and stability on the size of the perturbations.

A number of one-dimensional models have been developed to simulate (from parameterization) moist convective processes (e.g., Frank 1983; Clark and Arritt 1995; Kain and Fritsch 1990; Wetzel and Boone 1995; Stauffer et al. 1999). They have been used to simulate either shallow or deep convection, and a number of them have been incorporated into three-dimensional atmospheric models, for example, MM5 (e.g., Dudhia 1993). In three-dimensional models, they are usually used as cloud models, where triggering functions like those discussed above determine if convection occurs. In such cases, only grid-scale (resolved) PBL variables are retained, rather than for each individual parcel that can trigger convection. Rogers and Fritsch (1996) and Hong and Pan (1998) have tested their formulations in three-dimensional atmospheric models. Their results showed improvement when compared to simulations with triggering functions that did not include mesoscale fluctuations.

Lynn et al. (2001), Part I of this paper, used model output from a high-resolution, three-dimensional cloud-resolving model to simulate the atmospheric response to heating of west-to-east landscape patches. Their results suggested that rainfall varied linearly with the size of individual landscape patches; yet a number of small patches within a domain could produce more domain-averaged rainfall than one, relatively larger patch. Moreover, the magnitude of vertical velocity, temperature, and moisture in parcels occurring along sea-breeze-like fronts did not vary simply with patch size. For example, smaller patches could produce bigger parcel values than larger patches, especially when these smaller patches have a more appropriate ratio of local radius of deformation to patch size. The gradient in soil moisture, the background wind, atmospheric stability, and specific humidity, were among other variables that also affected the triggering variables within parcels. Lynn et al. (2001) used these variables (and others) to suggest dimensionaless numbers that could be used in a parameterization. These are, for example, the ratio of the local radius of deformation to the size of the patches (noted above), the ratio of gradient in the surface sensible heat fluxes to the mean surface sensible heat fluxes, the ratio of the background wind speed to a constant, light, background wind speed, and the ratio of the potential temperature difference between the free atmosphere and the planetary boundary layer to the mean temperature within the planetary boundary layer.

This paper uses the analysis of the high-resolution model results by Lynn et al. (2001) to develop new parameterizations for variables that can be used in the triggering of moist convection. There are at least two possible approaches to developing parameterizations for these triggering variables. The first of these possible approaches can use zero-order closure, while the second is first-order closure. The zero-order closure scheme is used to directly obtain the vertical profiles of *mesoscale* vertical wind, potential temperature, and specific humidity. Equation (1) in Part 1 is an example of a zero-order closure scheme. (Note, parameterizations have already been suggested for turbulent-scale triggering variables.) The parameterizations developed here could replace the formulas suggested by Rogers and Fritsch (1996) and Hong and Pan (1998), since they are based upon results from a high-resolution atmospheric model (and include variables such as background wind).

However, higher order closure models can provide more realistic simulation of atmospheric variables than simple zero-order schemes (e.g., Pielke 1984; Stull 1988), since they do not presuppose relationships between the independent and dependent variables. The first-order closure scheme used here requires budget equations to obtain the vertical profiles of the parcel's potential temperature and specific humidity. To reiterate, because the budget equations describe the actual, formal relationships between the independent and dependent variables, the first-order scheme should provide more realistic triggering variables than zero-order closure. Since these equations also contain source and sink terms, the differences obtained using zero- and first-order closure can be especially pronounced after moist convection occurs.

First-order closure can be used in the budget equation to obtain the vertical profiles of a parcel's potential temperature and specific humidity (including the mesoscale and turbulent contributions). It is suggested that the budget equations be incorporated into a one-dimensional (cloud) model. A combination of the budget equations (described below) and those equations currently used in cloud models can be used to describe the profile of temperature and moisture from the surface to cloud top.

In the next section, section 2, we suggest a new approach to the triggering of landscape-generated moist convection, by formally describing the set of budget equations that contain both mesoscale and turbulent fluctuations. In section 3, we present zero-order and first-order closure. The zero-order closure is straightforward (and uses similarity theory), but the first-order closure requires us to perform an analysis of the fluxes in the budget equations to show which need to be parameterized. Using similarity theory, we develop a parameterization for the necessary fluxes. A summary and conclusion is presented in section 4.

2. Method

a. Numerical model

Lynn et al. (2001) used a high-resolution, cloud-resolving model [the Goddard Cumulus Ensemble Model

TABLE 1. Variables required for parameterization. An analysis of the mesoscale kinetic energy showed that it had an *e*-folding time of 3 h (this *e*-folding time is used to calculate R_o).

Variable	Description	Units
L	Length scale of patch	m
R_o	Local radius of deformation	km
H	Planetary boundary layer height (for each dry patch)	m
H_c	Cloud-top Height	m
$\Delta w'''\theta'''$	Gradient of surface sensible heat fluxes	K m s^{-1}
Θ	Large-scale (Mean) planetary boundary layer temperature	K
$\Delta\theta$	Difference in potential temperature	K
Q	Large-scale specific humidity	
U	Large-scale, background wind	m s^{-1}
U_o^u	A function of patch size for parcels on upwind side of dry patch	m s^{-1}
U_o^d	A function of patch size for parcels on downwind side of dry patch	m s^{-1}
τ	Time	s

(GCE; Tao and Simpson, 1993)] to obtain their dataset (i.e., from model output). The reader is referred to their work for more details.

A number of simulation domains were used here, which are described by Lynn et al. (2001). Two in particular are discussed in detail. In Lynn et al.'s (2001) domain 1, there is a 64-km dry patch surrounded by two 32-km wet patches. Because the domain is periodic, there is actually a 64-km dry patch and 64-km wet patch in this domain. In domain 3, there were patches of (left to right) 7.5, 4, 16, 4, 8, 20, and 4 km in length. The relevant experiments that used the first domain were experiments 1 (light wind case), 6 (used observed wind), lw (light wind), and 8w (used observed wind). Experiment 3 used domain 3, and was produced using a light background wind. Simulations produced with moist processes turned on have a *w* after the experiment number. The names for each of the experiments listed here correspond to those in Tables 4a and 4b in Part I. We use the simulations with moist processes turned off to isolate the contribution of LGMCs in the PBL.

b. Parameterization

As shown by Lynn et al. (2001), the mesoscale triggering variables reach their maxima at different times during the simulation day, depending upon the patch size, soil moisture gradients, and large-scale environmental (background) conditions. Moreover, the mesoscale triggering variables have a different timescale than the turbulent triggering variables (Lynn et al. 1995a). This is because the mesoscale circulations develop in association with horizontal temperature gradients over patches that have length scales of 5–100 km, while turbulent circulations develop in association with vertical wind and temperature gradients within a PBL less than a few kilometers in height. Thus, to realistically describe the evolution of the triggering variables requires a prognostic equation for them, since the (turbulent) forcing of mesoscale circulations can change substantially during the life cycle of the mesoscale circulations. Similarity theory is used to obtain the relationships between the mesoscale triggering variables and various dimensionless numbers (Stull 1988).

Similarity theory uses various dimensionless numbers to obtain parameterizations for required variables. In our case, these variables are w'_o, θ'_o, and q'_o, a parcel's perturbation vertical velocity, potential temperature, and specific humidity. Here, the relevant variables used in the dimensionless numbers are shown in Table 1; many of them were mentioned in Lynn et al. (2001) as having an important effect on the triggering variables. They depend upon variables that can be obtained from the hosting model. Using dimensionless numbers to obtain the perturbations can be considered as a zero-order closure.

Alternatively, we can obtain a parcel's temperature and moisture from budget equations. These budget equations require that we obtain various fluxes also using information from the hosting (large-scale) model. They also require fluxes that consist of the correlation of subgrid-scale terms. Using similarity theory to obtain these fluxes can be considered first-order closure.

To produce budget equations for θ_s and q_s (subgrid-scale components of potential temperature and moisture), we write simplified equation for the perturbation ϕ_s, ignoring molecular diffusion (Stull 1988):

$$\frac{\partial\phi_s}{\partial t} + \tilde{U}_j\frac{\partial\phi_s}{\partial x_j} + u_{j,s}\frac{\partial\tilde{\phi}}{\partial x_j} + u_{j,s}\frac{\partial\phi_s}{\partial x_j} = \left\langle\frac{\partial u_{j,s}\phi_s}{\partial x_j}\right\rangle + S_{\phi_s}, \quad (1)$$

where the angle brackets indicate an average over a grid element of a large-scale model. We then rewrite in flux form to more simply obtain the required contributions. We assume that the horizontal advection of subgrid-scale quantities between grid elements in the large-scale model is small when compared to the vertical advection of these quantities. This is because we assume that circulations generated by patches are contained within each grid element of the hosting model; that is, the large-scale model:

$$\frac{\partial\phi_s}{\partial t} + \frac{\partial\tilde{w}\phi_s}{\partial z} + \frac{\partial w_s\tilde{\phi}}{\partial z} + \frac{\partial w_s\phi_s}{\partial z} = \left\langle\frac{\partial w_s\phi_s}{\partial z}\right\rangle + S_{\phi_s}. \quad (2)$$

TABLE 2. Miscellaneous definitions of variables (H is the planetary boundary layer height).

Variable	Definition
$\tilde{\phi}$	Large-scale average over domain of regional model
ϕ'	Mesoscale perturbation (horizontal scale > than $3H$)
ϕ''	Large eddy perturbation (250 m < horizontal scale ≤ $3H$)
ϕ'''	Small eddy perturbation (horizontal scale ≤ 50 m)
ϕ_s	Subgrid-scale perturbations obtained with GCE
ϕ_o	Average of ϕ over square area of parcel
$\overline{\phi}^p$	Same as ϕ_o

We then expand each term (but the first and last) by substituting for ϕ_s the mesoscale perturbation, ϕ'; the large eddy perturbation, ϕ''; and the small eddy perturbation, ϕ''' [see Lynn et al. (2001) for more details]. We have for each term:

$$\frac{\partial \tilde{w}\phi_s}{\partial z} = \frac{\partial \tilde{w}\phi'}{\partial z} + \frac{\partial \tilde{w}\phi''}{\partial z} + \frac{\partial \tilde{w}\phi'''}{\partial z}, \tag{3}$$

$$\frac{\partial w_s\tilde{\phi}}{\partial z} = \frac{\partial w'\tilde{\phi}}{\partial z} + \frac{\partial w''\tilde{\phi}}{\partial z} + \frac{\partial w'''\tilde{\phi}}{\partial z}, \tag{4}$$

$$\begin{aligned}\frac{\partial w_s\phi_s}{\partial z} = {} & \frac{\partial w'\phi'}{\partial z} + \frac{\partial w'\phi''}{\partial z} + \frac{\partial w'\phi'''}{\partial z} + \frac{\partial w''\phi'}{\partial z} \\ & + \frac{\partial w''\phi''}{\partial z} + \frac{\partial w''\phi'''}{\partial z} + \frac{\partial w'''\phi'}{\partial z} + \frac{\partial w'''\phi''}{\partial z} \\ & + \frac{\partial w'''\phi'''}{\partial z},\end{aligned} \tag{5}$$

$$\begin{aligned}\left\langle\frac{\partial w_s\phi_s}{\partial z}\right\rangle = {} & \left\langle\frac{\partial w'\phi'}{\partial z}\right\rangle + \left\langle\frac{\partial w'\phi''}{\partial z}\right\rangle + \left\langle\frac{\partial w'\phi'''}{\partial z}\right\rangle \\ & + \left\langle\frac{\partial w''\phi'}{\partial z}\right\rangle + \left\langle\frac{\partial w''\phi''}{\partial z}\right\rangle + \left\langle\frac{\partial w''\phi'''}{\partial z}\right\rangle \\ & + \left\langle\frac{\partial w'''\phi'}{\partial z}\right\rangle + \left\langle\frac{\partial w'''\phi''}{\partial z}\right\rangle + \left\langle\frac{\partial w'''\phi'''}{\partial z}\right\rangle.\end{aligned} \tag{6}$$

We can use the above equations to obtain θ_o and q_o, that is, a triggering parcel's potential temperature and specific humidity. This is done by substituting θ (and then q) for ϕ, and then averaging the equation for θ_o (and then q_o) over the area of a parcel. Note that

$$\phi_o = \overline{\phi'}^p + \overline{\phi''}^p + \overline{\phi'''}^p, \tag{7}$$

where the superscript p indicates an average over the area of the parcel. Table 2 provides a summary of definitions for ϕ, its various averages, and its perturbations.

We are able to simplify these equations for the purposes of this work. This is because Lynn et al. (2001) showed that the magnitude of mesoscale perturbations within parcels is constant over a wide range of area averages (see Fig. 8, Part 1). Therefore, $\overline{w'\phi'}^p + \overline{w''\phi'}^p = \overline{w_s\phi'}^p$ and other cross terms such as $\overline{w'\phi''}^p = 0$ (see Fig. 4 and Fig. 5). Moreover, by applying the Reynolds assumption the fluxes $\overline{\tilde{w}\phi'''}$, $\overline{w'''\phi}$, $\overline{w''\phi'''}$, and $\overline{w'''\phi''} = 0$. Then,

$$\frac{\partial\overline{\tilde{w}\phi_s}^p}{\partial z} = \frac{\partial\overline{\tilde{w}\phi'}^p}{\partial z} + \frac{\partial\overline{\tilde{w}\phi''}^p}{\partial z}, \tag{8}$$

$$\frac{\partial\overline{w_s\tilde{\phi}}^p}{\partial z} = \frac{\partial\overline{w'\tilde{\phi}}^p}{\partial z} + \frac{\partial\overline{w''\tilde{\phi}}^p}{\partial z}, \tag{9}$$

$$\begin{aligned}\frac{\partial\overline{w_s\phi_s}^p}{\partial z} = {} & \frac{\partial\overline{w_s\phi'}^p}{\partial z} + \frac{\partial\overline{w'\phi''}^p}{\partial z} + \frac{\partial\overline{w''\phi''}^p}{\partial z} \\ & + \frac{\partial\overline{w'''\phi'''}^p}{\partial z},\end{aligned} \tag{10}$$

$$\left\langle\frac{\partial w_s\phi_s}{\partial z}\right\rangle = \left\langle\frac{\partial w'\phi'}{\partial z}\right\rangle + \left\langle\frac{\partial w''\phi''}{\partial z}\right\rangle + \left\langle\frac{\partial w'''\phi'''}{\partial z}\right\rangle. \tag{11}$$

We note that the parameterized turbulent fluxes were large only in the lowest part of the PBL. This suggests that the cross terms that involve double (large eddy) and triple prime (small eddy) fluctations are indeed small above the lower PBL.

3. Results

a. Zero-order closure

To obtain the vertical profiles $w_o(z)$, $\theta_o(z)$, and $q_o(z)$ for each dry patch, Lynn et al. (2001), Part I, identified the location of the largest vertical velocity perturbation along each front over each side of the patch. This became the center of each parcel. For more details, the reader should refer to the discussion concerning Figs. 4 and 8 in their paper. The parcel chosen is the average of the GCE model grid-scale fields (which is the explicit simulation of the unresolved, subgrid-scale fields in a large-scale model), for w_s, θ_s, and q_s, over square areas of size about 5.1 km^2 (9 × 9 grid elements). This size is similar to observed cloud bases areas, and the area of cloud bases used in cumulus convection schemes.

The variables w'_o, θ'_o, and q'_o (here, referred to as X_i) are obtained from a prognostic equation:

$$\frac{dX_i}{d\tau} = \alpha_{X_i} D^1 D^2 D^3 D^{4\epsilon} Q^\gamma - \beta_{X_i} X_i, \tag{12}$$

where α_X and β_{X_i} are empirical parameters deduced from the numerical model output, and τ is linearly related to the time of day t. Here $\alpha_{w'} = 0.0012$ m s^{-1}, $\alpha_{w'_o}^{up} = 0.000\,54$ m s^{-1}, $\alpha_{\theta'_o} = 0.0017$ (K), and $\alpha_{q'_o} = 0.000\,16$ g kg^{-1}. Also, $\beta_{w'_o(\mathrm{down})} = 1/3600$, $\beta_{w'_o(\mathrm{up})} = 1/7200$, $\beta_{\theta'_o} = 1/3600$, and $\beta_{q'_o} = 1/10\,800$. $\gamma = 1$ for q'_o and zero otherwise; $\epsilon = 1$ for w_o and θ'_o and zero otherwise.

Note, the magnitude of the coefficients, $\alpha_{w'_o}$, $\alpha_{\theta'_o}$, and $\alpha_{q'_o}$ could depend on parcel size. We found, though, that the size of the parcel had only a very small effect on the magnitude of the triggering variables, since the mesoscale variables were not very sensitive to parcel size.

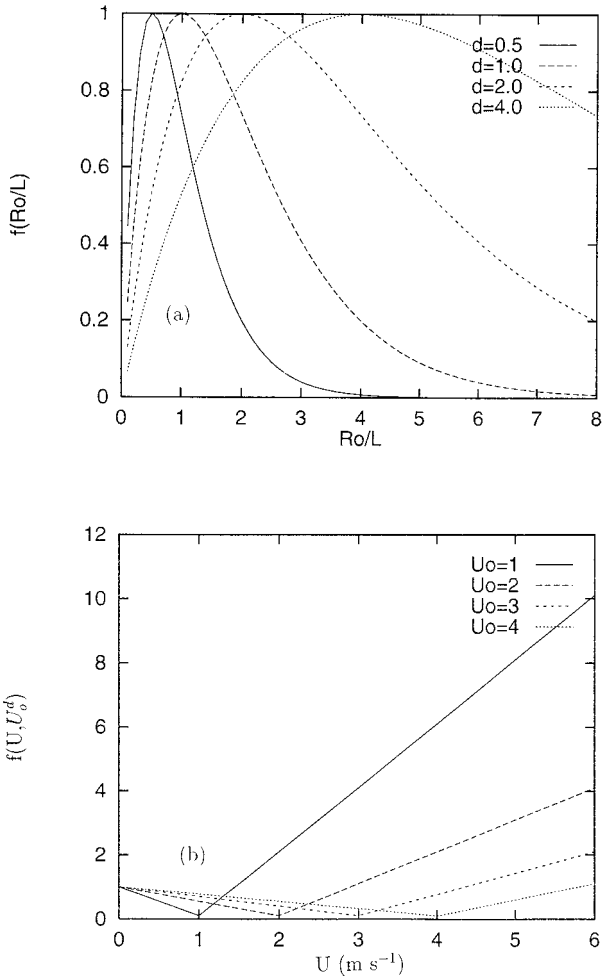

FIG. 1. (a) The variation of the function $f(R_o, L)$ with the coefficient d, where $f(R_o, L) = 2.718 \times e^{-dx}$, and $x = R_o/L$. (b) An example of the dependence of the function $f(U, U_o^d)$ on the parameter U_o^d, labeled simply as U_o in the legend. Both functions ''mimic'' those in the text, i.e., D^1 and D^2.

Therefore, the values of the α coefficients are probably valid for other parcel sizes than used here.

In regard to $\beta_{w_o'(\mathrm{down})}$ and $\beta_{w_o'(\mathrm{up})}$, they differ from each other because w_o' on the downward side of the patch occurs with a circulation opposing the prevailing wind, while w_o' on the upwind side of the patch requires the convergence of opposing circulatons to significantly increase in magnitude. Here $\beta_{\theta_o'}$ and $\beta_{q_o'}$ are different since the θ_o' reaches a maximum very closely following the heating of the PBL, while the q_o' reaches a maximum after significant transport of moisture into the upper PBL.

The triggering variables are determined by solving numerically Eq. (12) in two steps, using a ''time-splitting'' technique (e.g., Pielke 1984). In the first step, intermediate variables X_i^* are calculated using an explicit scheme:

$$X_i^*(\tau + \Delta\tau) = X_i(\tau) + \Delta\tau\alpha_{x_i}D^1D^2D^3D^4\epsilon Q^\gamma, \quad (13)$$

and in the second step, X_i is calculated using an analytical solution:

$$X_i(\tau + \Delta\tau) = X_i^*(\tau + \Delta\tau)e^{(-\Delta\tau\beta_{X_i})}. \quad (14)$$

For each function, we seek relationships that are robust, but simple to apply and ''modify'' if additional datasets suggest the need to do so.

The dimensionless number D^1 is ($x = R_o/L$, and L is greater than 5 km):

$$D^1_{w_o'} = xe^{-0.50x}, \quad (15)$$

$$D^1_{\theta_o'} = xe^{-0.50x}, \quad (16)$$

$$D^1q_o' = xe^{-0.50x}. \quad (17)$$

Figure 1a shows an example of this function for different values of the coefficients of x in the exponent of this function. [Note, Lynn et al. (1998) show how to obtain R_o.] When this function is a maximum, it indicates that conditions are optimal for the development of mesoscale circulations. When this function is less than the maximum, but increasing in value (to the ''left'' of the maximum), the circulations are developing toward their peak mesoscale kinetic energy. Beyond the maximum, the decrease in the function indicates that the circulations are in the process of dissipating.

In regard to the dimensionless number D^2, it represents the impact of wind on parcels on the upwind and downwind of the center of the dry patch. For parcels generated on the downwind side of the patch:

$$D^2_{w_o'} = \begin{cases} 1.0 - 0.25\dfrac{U}{U_o^d} & U - U_o^d < 0 \\ 0.75 + 0.5\dfrac{U - U_o^d}{U_o^d} & U - U_o^d > 0, \end{cases} \quad (18)$$

$$D^2_{\theta_o'} = \begin{cases} 1.0 - 0.1\dfrac{U}{U_o^d} & U - U_o^d < 0 \\ 0.9 + 2.0\dfrac{U - U_o^d}{U_o^d} & U - U_o^d > 0, \end{cases} \quad (19)$$

$$D^2_{q_o'} = \begin{cases} 1.0 - 0.1\dfrac{U}{U_o^d} & U - U_o^d < 0 \\ 0.9 + 1.75\dfrac{U - U_o^d}{U_o^d} & U - U_o^d > 0. \end{cases} \quad (20)$$

For patches generated on the upwind side of the patch, the equations and coefficients are different than above:

$$D^2_{w_o'} = \left\{ 1.0 + 0.15\frac{U - U_o^u}{U_o^u} \quad U - U_o^u > 0, \right. \quad (21)$$

$$D^2_{\theta_o'} = \begin{cases} 1.0 - 0.3\dfrac{U}{U_o^{u,\theta}} & U - U_o^{u,\theta} < 0 \\ 0.7 + 0.9\dfrac{U - U_o^{u,\theta}}{U_o^{u,\theta}} & U - U_o^{u,\theta} > 0, \end{cases} \quad (22)$$

$$D^2_{q'_o} = 1.0 + 0.15\frac{U - U^u_o}{U^u_o}. \quad (23)$$

Here, U is the mean background (a large-scale model's, grid-scale resolved) wind (always positive), and U^d_o (downwind) and U^u_o (upwind) are the background wind at which the maximum triggering variables were obtained. The background wind (in the PBL) was about 2.5 m s^{-1} when the maxima of the triggering variables were obtained over a 64-km patch. To simplify the application of these results to the parameterization, we simply assume that $U^d_o = 0.5 + 3.125 \times 10^{-5}$ s^{-1} L (=2.5 m s^{-1} for a 64-km patch.). In regard to U^u_o, it equals 0.5 m s^{-1}. For the parameter $U^{u,\theta}_o$, we suggest $U^{u,\theta}_o = 9.375 \times 10^{-5}$ s^{-1} L (=6.0 m s^{-1} for a 64-km patch.). The difference in these two parameters occurs because of the effect of background wind on the circulations on each side of a dry patch.

For example, Fig. 1b shows the dependence of $D^2(U, U^d_o)$ upon U^d_o for a set of coefficients. Note, that $D^2(U, U^d_o)$ decreases from a value of 1 with increasing U^d_o until $U = U^d_o$. It then increases with increasing U. The purpose is to represent the impact of background wind on the temperature gradient on either the upwind or downwind side of the patch, with changing background wind. That is, there is a value of U such that the trigger function variables are a maximum. When this function is far to the left of its minimum, the wind speed is too light to aid in the development of mesoscale circulations on the downwind side of the patch. In this case, there is relatively little effect of wind speed on the atmospheric, horizontal temperature gradients. In comparison, as the wind speed increases, this D^2 increases, indicating that the background wind is causing the horizontal temperature gradients to dissipate.

The dimensionless number D^3 is

$$D^3 = \frac{\Delta w'''\theta'''}{\langle w'''\theta'''\rangle}, \quad (24)$$

where these are the parameterized surface heat fluxes. To represent the residual impact of the heat fluxes on the PBL, the numerator and denominator of D^3 each have an e-folding time of 3 h. An increase in this dimensionless number would indicate that the forcing on the mesoscale heat fluxes is also increasing. Here, though, we are most concerned with changes in this number as the gradient of the heat fluxes changes with changing soil moisture or vegetation.

The variable $\Delta\theta$ is the difference in temperature between the free atmosphere and mean of the PBL temperature Θ (this difference is taken between the temperature that is located 1000 m above the top of the PBL and the mean temperature of the PBL). Note, the ratio of R_o/L accounts for the most part of the sensitivity of the parameterization to stability, especially from anytime within any particular day. To parameterize the triggering variables w_o and θ'_o, there was needed an additional dimensionless variable:

$$D^4_{w'_o} = 1 - 8.0\frac{\Delta\theta}{\Theta}, \quad (25)$$

$$D^4_{\theta'_o} = 1 + 18.0\frac{\Delta\theta}{\Theta}. \quad (26)$$

The dimensional variable Q is simply the PBL mean specific humidity.

We used model output to obtain the complete set of dimensionless numbers, and parameterized curves. We used all of the simulations with moist processes turned off, and one with moist processes turned on (experiment lw). For example, Fig. 2 shows the parameterized curves for each triggering variable for experiment 1 (64-km patch) and experiment 3 (for the 8- and 20-km patches). Also shown are the results for experiment lw (64-km patch with moist processes turned on). Figure 3 shows the maximum from the parameterized curves for a range of patch sizes and background winds. These figures can be compared to those shown in Lynn et al. (2001) (i.e., Figs. 7, 10, and 11). This comparison demonstrates the ability of the parameterization to represent the sensitivity of the model results to patch size and wind. To quantitatively evaluate the parameterization, we calculated the mean and resulting absolute difference. The mean for w'_o was 0.27 m s^{-1}, while the absolute difference was 0.13 m s^{-1}. The mean for θ'_o was 0.57 K and the absolute difference was 0.26 K, while the mean for q'_o was 1.28 g kg^{-1} and the absolute difference was 0.48 g kg^{-1}. All variables varied irregularly in time, leading to much of the absolute difference between the modeled output and the parameterization.

To compare the datasets in another, perhaps, better way, we calculated the integral of the parameterization versus the model results. The parameterized w'_o was 17% larger than the model results, while θ'_o was 18% larger, and q'_o 13% larger. Excluding the time after which the PBL collapsed, that is, the last 2 h of modeled data, the numbers were 14%, 17%, and 7%. Some of the difference between the parameterization and the model results occurred because it was assumed that dissipation can be represented by a constant, β. Yet, β could be modeled as a function of variables such as wind and stability, although we chose not to do for reasons of simplicity. In summary, the parameterization captured the most important features of the model output: that is, changes in the mesoscale contribution to the triggering variables owing to their (i) dependence of each variable upon patch size, (ii) background wind (upwind and downwind side of dry patch), (iii) gradient in soil moisture, (iv) stability, and (v) specific humidity.

b. *First-order closure*

The budget equations contain a number of different fluxes, some of which already have parameterizations in the literature. These are the turbulent fluxes and mesoscale fluxes. Before obtaining new parameterizations

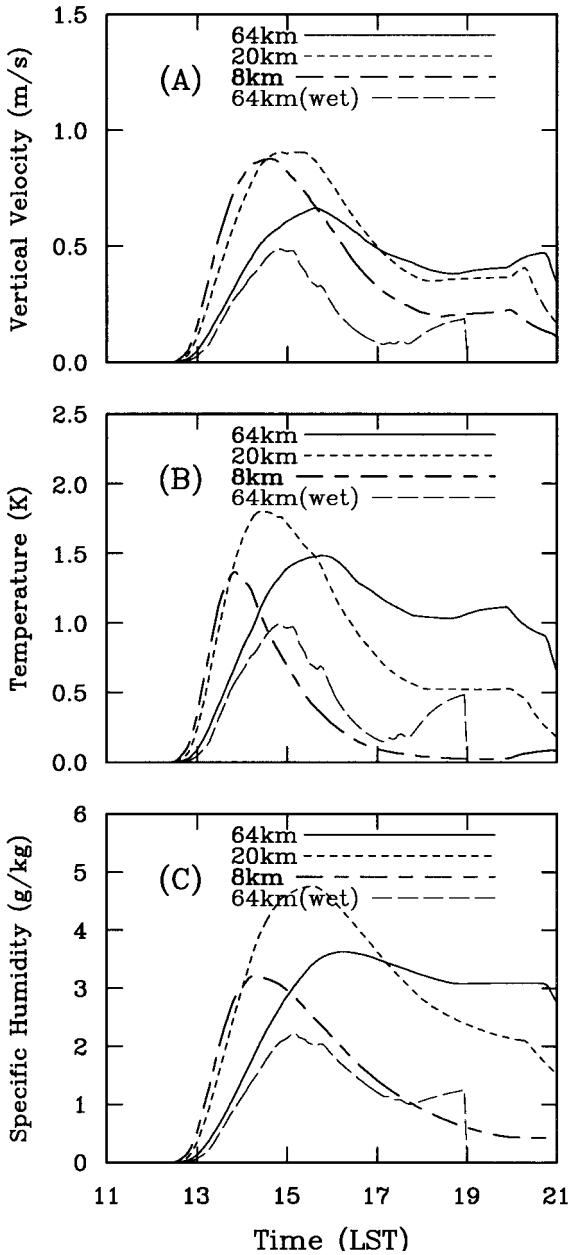

FIG. 2. Time dependence of triggering variables obtained from the parameterization, for experiments 1, 3 (20 and 8-km patches), and 1w.

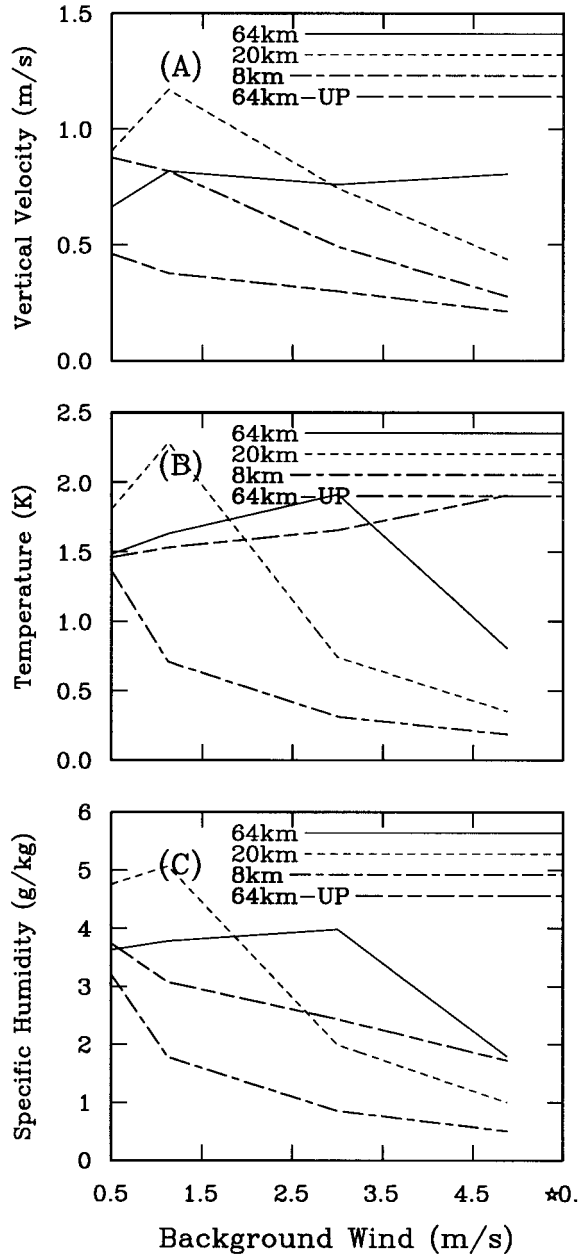

FIG. 3. The maximum value for the variables (a) w'_o, (b) θ'_o, and (c) q'_o, obtained in experiments 1, 3, and 5–10, for the wind speeds shown, using the parameterization for each of these variables.

for any of the other flux terms in the budget equations, it is prudent to determine which of them contribute most to the total flux. We will ignore those fluxes whose contributions are small.

The fluxes presented below were calculated using parcels with the same areas described above. To find the flux $\overline{\tilde{w}_s\theta}^p$ in Eq. (8), one needs to find $\overline{\phi_s}^p$, but $\overline{\phi_s}^p = \phi_o$, which is a solution to the budget equations. To find the flux $w_s\tilde{\theta}^p$ in Eq. (9), one is required to obtain w'_o and w''_o. Lynn et al. (2001) presented an empirical relationship for w'_o, while Rogers and Fritsch (1996) suggest how to obtain w''_o from the turbulent kinetic energy, with $w'_o + w''_o = w_o$ or w_s. This leaves a number of unknowns in Eqs. (10) and (11).

Figure 4 shows the vertical profiles of the vertical flux of mesoscale temperature and moisture ($\overline{w_s\theta'}^p$ and $\overline{w_sq'}^p$), the vertical flux of the turbulent perturbations by the mesoscale wind ($\overline{w'\theta'}^p$ and $\overline{w'q'}^p$), the large-eddy turbulent fluxes $\overline{w''\theta''}^p$ and $\overline{w''q''}^p$), and the large-scale model's grid-scale mesoscale fluxes ($\langle w'\theta'\rangle$ and $\langle w'q'\rangle$). The profiles were obtained from experiment 6.

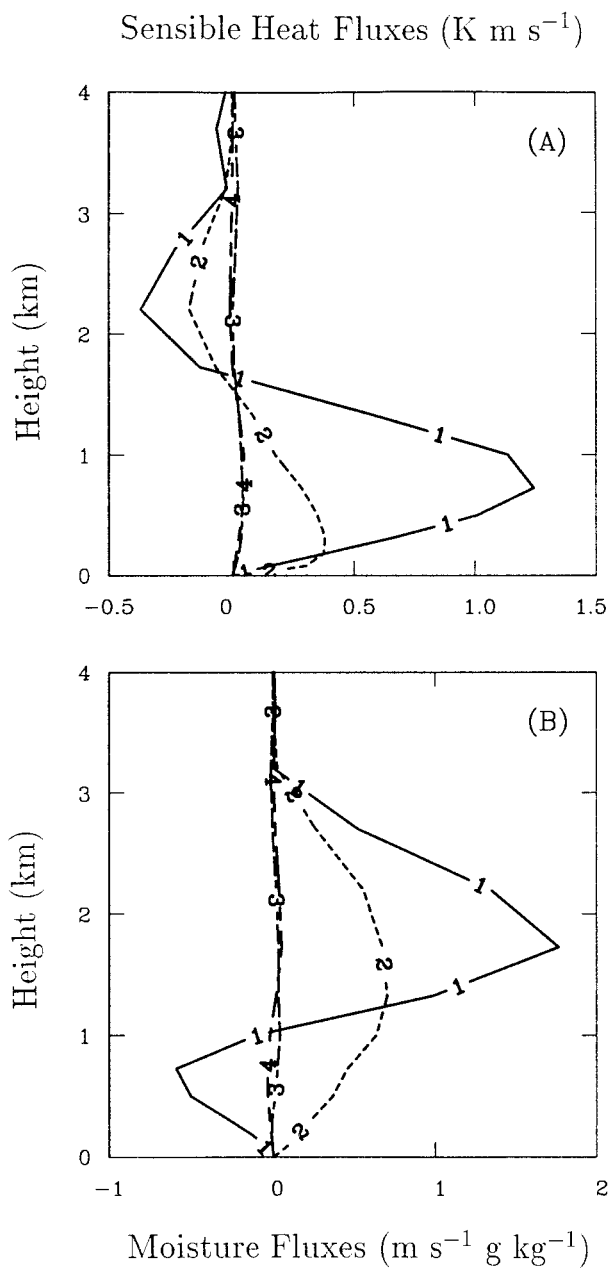

FIG. 4. Vertical profile of (a) heat and (b) moisture fluxes obtained in experiment 6. The labels on the profiles in (a) correspond as follows: 1) $\overline{w_s\theta'}^p$, 2) $\overline{w''\theta''}^p$, 3) $\overline{w'\theta''}^p$, and 4) $\langle w'\theta'\rangle$. The labels on the profiles in (b) correspond as follows: 1) $\overline{w_sq'}^p$, 2) $\overline{w''q''}^p$, 3) $\overline{w'q''}^p$, and 4) $\langle w'q'\rangle$. The overline with a superscript p indicates an average over the area of the parcel (note: this area is much smaller than the area of the simulation domain; the parcel mesoscale fluxes are correspondingly much larger than the grid-averaged fluxes). These fluxes are among those shown in Eqs. (9) and Eqs. (10), and were obtained from the high-resolution model output. Note, flux 3 is a ''cross term'' from Eq. (5). It is indeed small, as postulated in section 2b. Moist processes were turned off in these experiments.

We chose experiment 6 because it used the observed sounding (with the u wind), which is, perhaps, more typical than a light-wind case (experiment 1). Most importantly, Fig. 4 shows that $\overline{w_s\phi'}^p$ is much larger than $\overline{w''\phi''}^p$ (the large eddy flux), and has different vertical structure. This shows that the former contributes quite signficantly to the parcel's temperature and moisture profile, and should be included in the budget equations. Thus, there is a need to develop a parameterization for $\overline{w_s\theta'}^p$ and $\overline{w_sq'}^p$. However, we need not develop parameterizations for $\overline{w'\theta''}^p$ or $\overline{w'q''}^p$, nor include the grid-scale mesoscale fluxes, since they do not contribute significantly to the total flux. Parameterizations already exist for the turbulent fluxes.

Figure 5 shows the vertical profiles of the fluxes in the budget equations for those obtained in experiment 8w (moist processes turned on, with the observed wind used to initialize the model). An examination of this figure suggests the following: (i) Both $\overline{w_s\theta'}^p$ and $\overline{w_sq'}^p$ again significantly contribute to the structure of PBL variables. (ii) The heat flux $\overline{w_s\theta'}^p$ has a self-similar[1] profile, meaning that a parameterization for it can be simply developed for use prior to and during moist convection. (Thus, a parameterization developed for it using a simulation with moist processes turned off should apply for cases turned on.) (iii) Cumulus parameterizations used in large-scale models can be used to determine the vertical profile of $\overline{w''\theta''}^p$ within the cloud.

The heat flux $\overline{w_sq'}^p$, however, only exhibits a self-similar profile below 2 km in height. In fact, this flux contributed to the vertical flux of moisture within the cloud (above 2 km with the cloud base near 1.5 km), in response to the occurance of moist processes. However, the mesoscale vertical velocity, w'_o, (Fig. 9 in Part 1) was very small above 2 km. Therefore, $\overline{w_sq'}^p$ is approximately equal to $\overline{w''q'}^p$ above 2 km. Then, the total flux within the cloud is $\overline{w''q'}^p + \overline{w''q''}^p$, which equals $\overline{w_sq_o}$ (when w'_o is small). This flux is already calculated using cumulus parameterization schemes. Therefore, it is probably reasonable to calculate $\overline{w_sq'}^p$ using the parameterization presented in this section, recognizing that cumulus parameterization schemes already include the contribution from moist processes.

Note, unlike the results for $\overline{w_sq'}^p$, moist processes did not affect the vertical structure of the mesoscale heat fluxes (although the magnitude changed). Therefore, these curves (for mesoscale fluxes) are self-similar prior to and during moist convection, and parameterizations developed prior to here for these fluxes should work in both dry and moist regimes (Lynn et al. 1995a; Zeng and Pielke 1995). These fluxes can affect moist convection indirectly, by their influence on the large-scale models, grid-scale variables.

[1] A profile whose vertical shape does not change with changes in the magnitude of the profile.

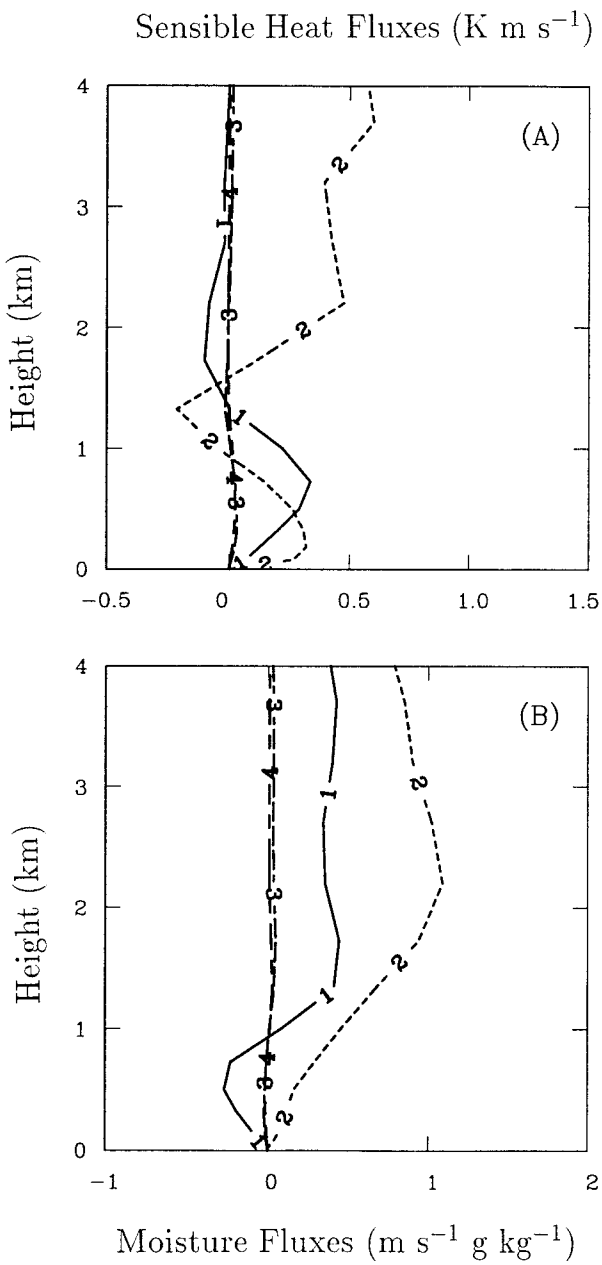

FIG. 5. Same as Fig. 4 but for experiment 8w. Moist processes were turned on in this experiment, and the simulation was run for 12 h.

The results obtained above were found to apply to other experiments (Part 1) produced as part of this work. Therefore, we believe the conclusions reached to be valid for initial conditions other than those examined here. Note, we do not show in any of our figures the grid-scale-averaged turbulent large eddy and small eddy fluxes. Nor, do we show the vertical profiles of the source terms, S_{θ_s} or S_{q_s}. We found, though, that each should be included in the budget equations. A summary of terms required in the budget equations are in Table 3.

TABLE 3. Budget equations terms. An X in the appropriate column indicates that the corresponding term needs to be included in its particular budget equation. A $\surd$ indicates that an appropriate parameterization needs to be developed for that term; otherwise, parameterizations exist for that indicated term in the literature. The angle brackets indicate an average over the large-scale grid of the hosting model. The $\overline{\phi}^p$ indicates an average over the area of the triggering parcel, where $\phi_o = \overline{\phi'}^p + \overline{\phi''}^p + \overline{\phi'''}^p$. The variable ϕ' is the mesoscale perturbation, while the variable ϕ'' is the large eddy, turbulent perturbation. The variable ϕ''' is the small eddy turbulent turbulent perturbation. See Eqs. (10) and (11).

Term	Include	Develop parameterization
$\langle w'\theta' \rangle$		
$\langle w''\theta'' \rangle$	X	
$\langle w'''\theta''' \rangle$	X	
$\overline{w_s\theta'}^p$	X	$\surd$
$\overline{w''\theta''}^p$	X	
$\overline{w'\theta''}^p$		
$\overline{w'''\theta'''}^p$	X	
$\langle w'q' \rangle$		
$\langle w''q'' \rangle$	X	
$\langle w'''q''' \rangle$	X	
$\overline{w_sq'}^p$	X	$\surd$
$\overline{w''q''}^p$	X	
$\overline{w'q''}^p$		
$\overline{w'''q'''}^p$	X	
S_θ	X	
S_q	X	

The structure of the curves shown in Figs. 4 and 5 evolved in time and changed with background wind. Figure 6 shows the vertical profile of $\overline{w_s\theta'}^p$ for experiments 1, 6, lw, and 3, for four, 3-hourly periods. As a reminder to the reader, we note that each of the first three listed experiments had a 64-km patch, but in experiment 1 the wind was a light background wind; in experiment 6, the observed wind profile was used; and experiment lw had moist processes turned on with a light (u) background wind. In experiment 3, we show results for the 8-km patch (at a light wind speed). Experiment 6 had the largest maxima, which pertains to the experiment with the observed wind speed. This was larger than in other cases, and occurred because of the effect of a background wind on atmospheric temperature gradients (Pielke 1984). Note, the shape of some of the the curves also evolved differently in time. For example, the minimum value in $\overline{w_s\theta'}^p$ in experiment 3 was larger than the maximum in the same experiment unlike, for example, experiment 1. This occurred because of the collision of the mesoscale circulations over the center of the 8-km patch. This caused the circulations to advect more cool air off the surrounding vegetation than before this collision.

Figure 7 shows the vertical profile of $\overline{w_sq'}^p$ for the same experiments as Fig. 6. These curves evolved differently with patch size and wind shear/speed. As described by Lynn et al. (1998), wind shear can affect the "tilt" and shape of LGCMs. Therefore, it is not surprising that the vertical structure of the fluxes can change with wind shear, as the ascending parcel is dis-

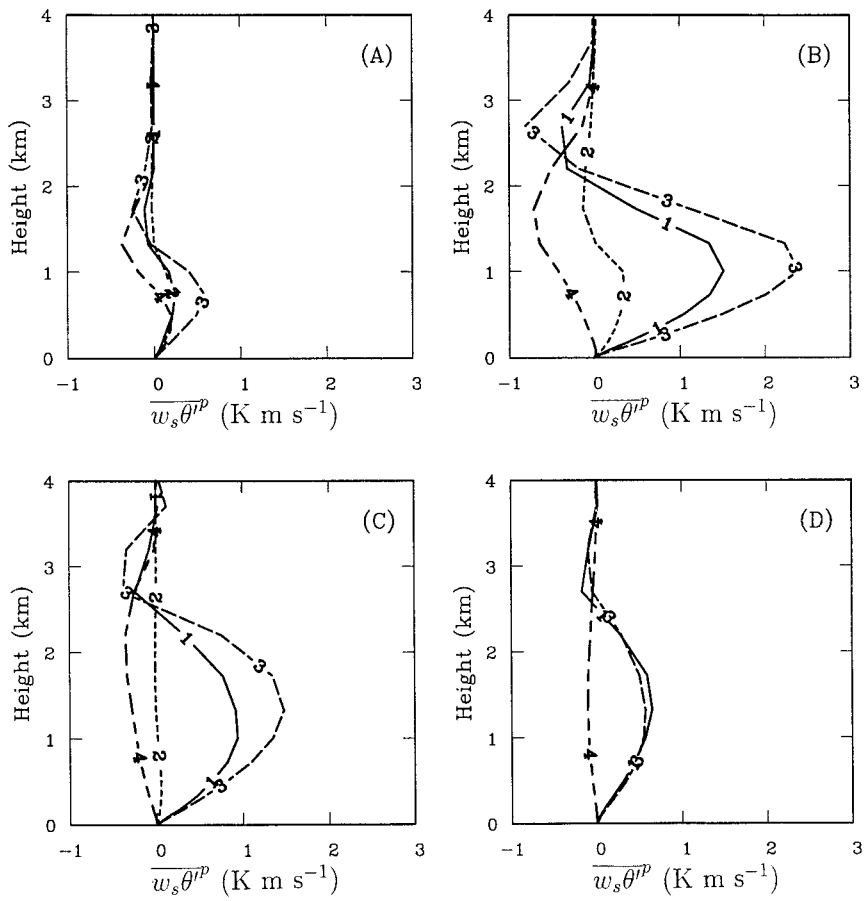

FIG. 6. Three-hour averages of $\overline{w_s\theta'}^p$ obtained in experiments 1 (labeled 1), 1w (labeled 2), 6 (labeled 3), and 3 (8-km patch, labeled 4) between (a) 0900 and 1200 LST, (b) 1200 and 1500 LST, (c) 1500 and 1800 LST, and (d) 1800 and 2100 LST.

placed more toward the center of the dry patch (especially since there is a very tight moisture gradient along the sea-breeze-like fronts). The convergence of circulations over the center of the dry patch in experiments 3 and 6 also affected the profile of $\overline{w_s q'}^p$. For example, the shape of the curve in experiment 6 evolves from a fourth-order polynome to something more similar to a second-order polynome. This was, as above, due to the vertical advection of cool, moist air off the vegetation. Moist convection also affected in experiment lw the vertical structure of the curve $\overline{w_s q'}^p$. The development of a cold pool of air behind the sea-breeze-like fronts also affected the tilt of the circulations. This too led to a displacement of the ascending air parcel to be over the driest air above the dry patch.

Figure 8 shows that patch size and moist convection affected the time dependence of the maxima in the vertical profiles of the sensible heat fluxes, $\overline{w_s\theta'}^p$. In a simple sense, this is because the ratio of R_o/L was reached later in the simulation period (when the PBL was more developed) over the larger patches. In comparison, patch size affected most strongly the timing in the maxima of $\overline{w_s q'}^p$, but not the maxima itself. This can be explained by greater advection of moisture into the LGCMs of smaller patches, since the moist patch edges are closer to the center of the domain. This led to larger perturbations in moisture over the center of the smaller 8-km patch. Experiment 1 produced larger maxima than experiment 1w, since cloud cover reduced the solar radiation incident at the land surface.

To show how each of the relevant budget terms varied with wind speed, Fig. 9 shows the maximum from curves obtained for four different wind speeds [i.e., from experiments 1, 3, 5–10 in Lynn et al. (2001)]. Three different patch sizes are shown for this figure: 64, 20, and 8 km. For each patch size and curve, there is a wind speed at which the maximum occurs. This wind speed is largest for the 64-km patch and smallest for the 8-km patch. Thus, one should not ignore the triggering of moist convection by larger patches of moderate wind speed. Moreover, the results suggest that the contribution of the mesoscale fluxes to the subgrid-scale fluxes in large-scale models can be important at both low and high wind speed, depending upon patch size.

A number of simulations were also produced by Lynn

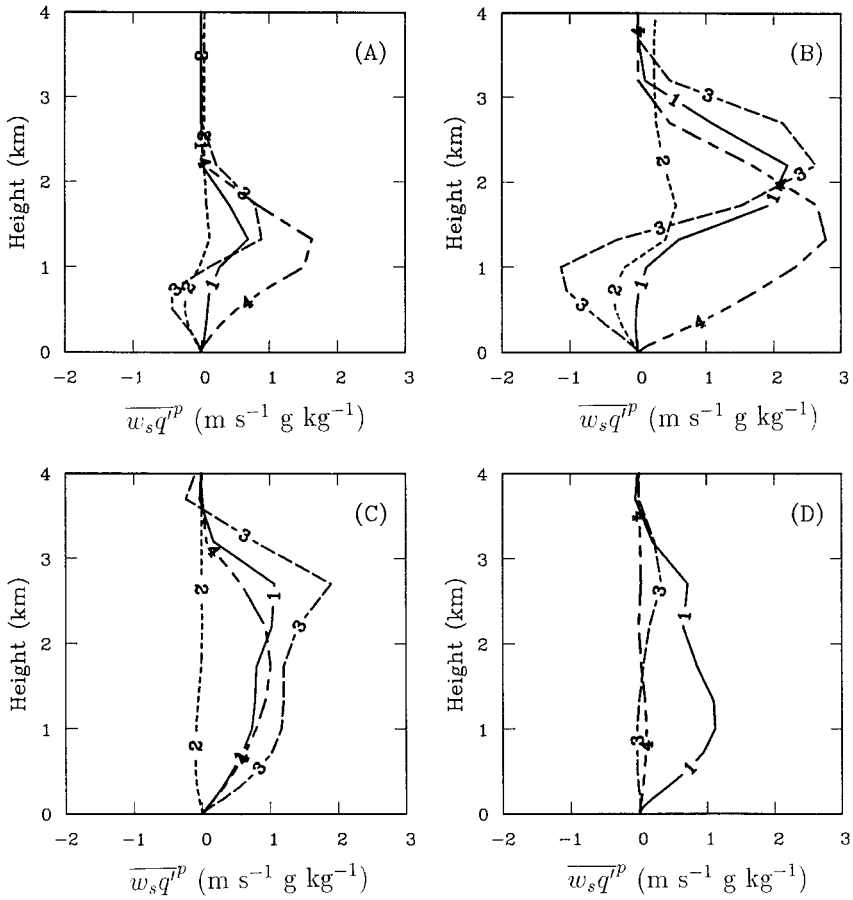

FIG. 7. The same as Fig. 6 but for $\overline{w_s q'^p}$.

et al. (2001) to examine the effect of stability, soil moisture gradients, and specific humidity. In regard to changes in static stability, the profiles of the flux terms had smaller magnitude when the static stability increased. The same profiles vary linearly in magnitude with changes in sensible heat fluxes associated with changes in soil moisture gradient or with changes in mean PBL specific humidity. Lynn et al. (2001) showed that the vertical depth and magnitude of the triggering variables corresponded to the magnitude of rainfall over patches of different sizes. Thus, parameterizations developed for the budget equations need also to be sensitive to these variables.

Finally, Lynn et al. (2001) examined the effect of parcel size on the triggering variables. They found that the profile of the triggering variables θ_o and q_o was relatively insensitive to parcel size. Therefore, the parameterization developed below should be valid for different parcel sizes.

To obtain the profiles of the fluxes, we first averaged them over 3-h periods and normalized each by its maximum. The advantage of this is that these (fourth-order polynomial) dimensionless curves can then be described by a set of coefficients, whose values can be given in a table. Then, it is only necessary to parameterize the maximum value for each curve, rather than five coefficients for each. A Chebyshev polynomial has been used to describe the vertical structure of the relevant terms in the budget equations. Therefore, we obtained coefficients for a Chebyshev polynomial.

Note, however, that the coefficients for $\overline{w_s \theta'^p}$ vary in time. The coefficients for $\overline{w_s q'^p}$ also vary in time, but with changes in the mean wind U and because of moist convection. To account for the possible time dependence of the coefficients we use various dimensionless numbers with a list of coefficients (for the polynome) that are given in Tables 4a and 4b. Otherwise, the maximum in the vertical profile of the two fluxes (here, referred to as X_i) are obtained from a prognostic equation:

$$\frac{X_i}{d\tau} = -\alpha_{X_i} D^1 D^5 Q^\gamma - \beta_{X_i} X_i. \tag{27}$$

Here, $\alpha_{\overline{w_s\theta'^p}} = 0.0041$ K m s^{-1} and $\alpha_{\overline{w_s q'^p}} = 0.020$ g kg^{-1} m s^{-1}. The dissipation $\beta_{\overline{w_s\theta'^p}} = 1/10\,800$, and $\beta_{\overline{w_s q'^p}} = 1/10\,800$. Here $\gamma = 1$ for $\overline{w_o q'^p}$ and zero otherwise. Note, the dissipation time (10 800 s) of the fluxes cor-

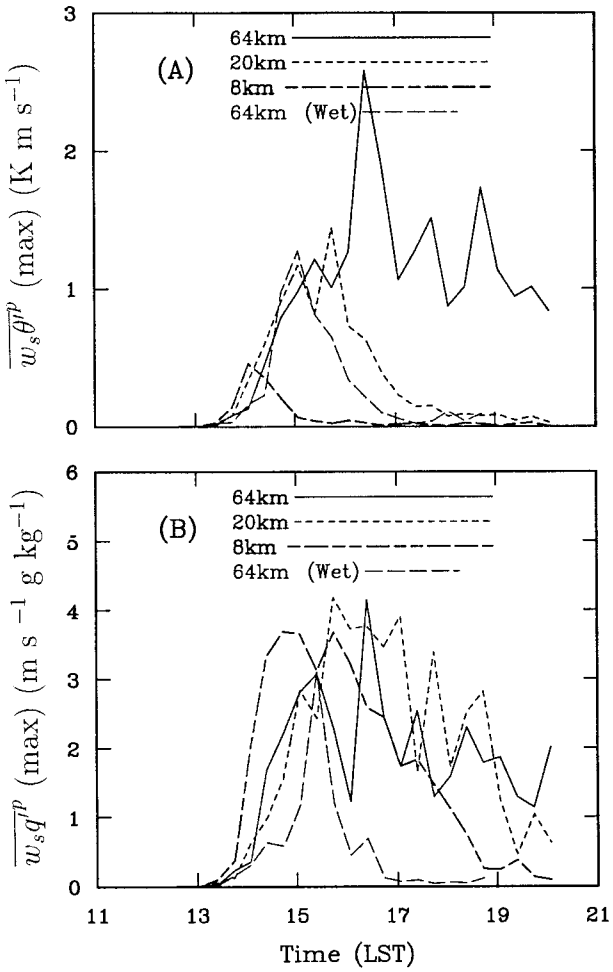

FIG. 8. The time dependence of (a) $\overline{w_s\theta'^p}$(max) and (b) $\overline{w_sq'^p}$(max) for experiments 1 and 1w (64-km patch) and the patches shown in experiment 3. The ''max'' indicates that the graphs show the maximum flux from each curve at the time shown.

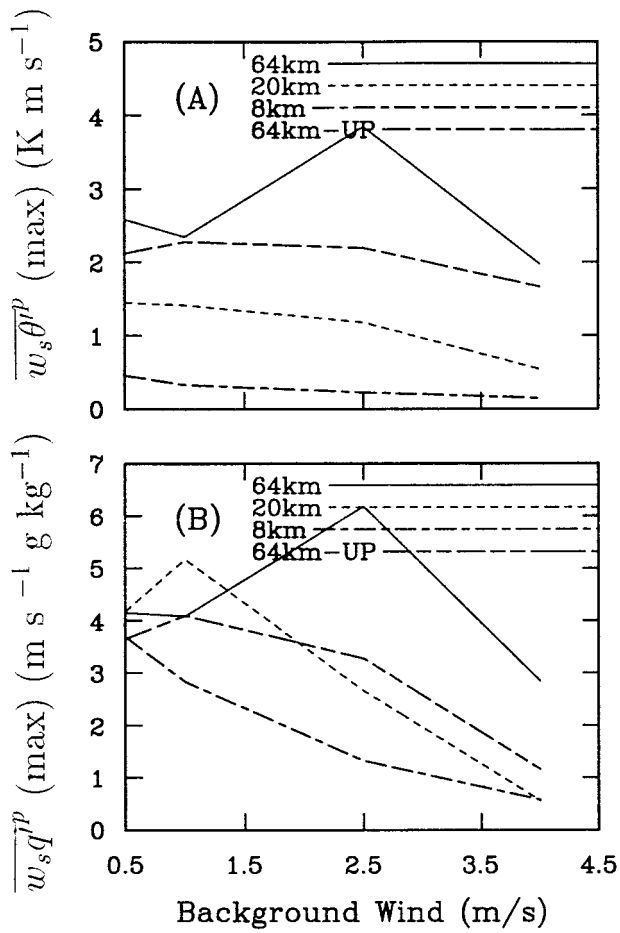

FIG. 9. The maximum value from the profile of the indicated fluxes obtained during experiments along the downwind (and upwind—UP) side of the dry patches for the sizes and and wind speeds shown.

responds to the dissipation of the mesoscale kinetic energy.

The triggering variables are determined by solving numerically Eq. (27) in two steps, again using a ''time-splitting'' technique (e.g., Pielke 1984). In the first step, intermediate varibles X_i^* are calculated using an explicit scheme:

$$X_i^*(\tau + \Delta\tau) = X_i(\tau) + \Delta\tau\alpha_k D^1 D^5 Q^\gamma, \qquad (28)$$

and in the second step, X_i is calculated using an analytical solution:

$$X_i(\tau + \Delta\tau) = X_i^*(\tau + \Delta\tau)e^{(-\Delta\tau\beta_{X_i})}. \qquad (29)$$

For each function, we seek relationships that are robust, but simple to apply and ''modify'' if additional datasets suggest the need to do so.

TABLE 4a. Coefficients for the Chebyshev polynomial $\overline{w_a\theta'^p}$. Here $D_L = R_o/L$. These curves are no larger than 0.1, when $\hat{z} >$ greater than the PBL height. The maximum for each of these curves should equal 1.

D_L	c_1	c_2	c_3	c_4	c_5
$0.00 \le D_L < 0.33$	0.316	−0.363	−0.002	0.434	−0.180
$0.33 \le D_L < 0.66$	0.406	−0.271	0.001	0.304	−0.270
$0.66 \le D_L < 1.00$	0.492	−0.306	−0.085	0.363	−0.196
$1.00 \le D_L < 1.33$	0.484	−0.291	−0.148	0.380	−0.119
$1.33 \le D_L < 1.75$	0.457	−0.319	−0.039	0.362	−0.212
$1.75 \le D_L < 3.00$	0.265	−0.284	0.191	0.317	−0.411
$3.00 \le D_L < 6.00$	−0.189	−0.242	0.803	0.308	−0.767
$6.00 \le D_L < 9.00$	−32.892	10.566	26.013	−14.969	−10.549
$9.00 \le D_L < 12.00$	−197.173	80.836	109.856	−103.523	−18.064

TABLE 4b. Coefficients for the Chebyshev polynomial $\overline{w_s q'^p}$ $D_{\text{sum}} = D_{\text{U}} - D_{U_v} - D_c$, where $D_{\text{U}} = \sum_{\tau=1}^{\tau=N} 3.0\text{U}\Delta\tau/\text{L}$, $D_{U_\phi} = U/0.5[\text{m s}^{-1}]$, and $D_c = H_c/H, -1$ ($D_c > 0$). Note, $U > 0.5$ m s^{-1}. These curves are equal to zero at $\hat{z} = 0$ and no smaller than 0.0 when $\hat{z} > 1.0$. The maximum for each of those curves should equal 1.

D_{sum}	c_1	c_2	c_3	c_4	c_5
$-8.00 \le D_{\text{sum}} < -5.00$	0.043	0.341	−0.263	−0.474	0.290
$-5.00 \le D_{\text{sum}} < -3.50$	0.114	0.064	−0.307	−0.059	0.355
$-3.50 \le D_{\text{sum}} < -2.75$	0.282	0.216	−0.336	−0.308	0.266
$-2.75 \le D_{\text{sum}} < -1.50$	0.284	−0.033	−0.344	0.053	0.280
$-1.50 \le D_{\text{sum}} < -0.50$	0.407	0.019	−0.363	−0.076	0.188
$-0.50 \le D_{\text{sum}} < -0.25$	0.316	−0.064	−0.333	0.104	0.236
$-0.25 \le D_{\text{sum}} < 0.00$	0.501	−0.163	−0.325	0.178	0.115
$0.00 \le D_{\text{sum}} < 0.25$	0.699	−0.268	−0.327	0.285	−0.050
$0.25 \le D_{\text{sum}} < 3.00$	0.521	−0.129	−0.454	0.123	0.207
$3.00 \le D_{\text{sum}} < 5.00$	0.589	−0.235	−0.346	0.289	0.056
$5.00 \le D_{\text{sum}} < 7.00$	0.607	−0.270	−0.290	0.331	−0.004
$7.00 \le D_{\text{sum}} < 9.00$	0.712	−0.167	−0.329	0.327	0.111

The dimensionless number D^5 is

$$D^5_{\overline{w_s\theta'}^p} = \frac{\Delta w'''\theta'''}{[\text{m s}^{-1}]f(U, U_o)[K^{0.5}]\Delta\Theta^{0.5}}, \tag{30}$$

$$D^5_{\overline{w_s q'}^p} = \frac{\Delta w'''\theta'''}{[\text{m s}^{-1}]f(U, U_o)\Delta\Theta}, \tag{31}$$

where K is a unit Kelvin. Lynn et al. (1995a) discuss how a dimensionless variable very similar to this one varies as a function of time of day, soil moisture gradient, background wind, and stability.

In regard to the dimensionless number $f(U, U_o)$, it represents the impact of wind on parcels on the upwind and downwind of the center of the dry patch. This is very similar to D^2 above. For parcels generated on the downwind side of the patch:

$$f(U, U_o^d)_{\overline{w_s\theta'}^p} = \begin{cases} 1.0 - 1.0 - 0.037(L\ [\text{m}^{-1}\ \text{s}])^{0.25}\dfrac{U}{U_o^d} & U - U_o^d < 0 \\ 1.0 - 0.037(L\ [\text{m}^{-1}\ \text{s}])^{0.25} + 0.5\dfrac{U}{U_o^d} & U + U_o^d \ge 0, \end{cases} \tag{32}$$

$$f(U, U_o^d)_{\overline{w_s q'}^p} = \begin{cases} 1.0 - 0.006(L\ [\text{m}^{-1}\ \text{s}])^{0.33}\dfrac{U}{U_o^d} & U - U_o^d < 0 \\ 1.0 - 0.0060(L\ [\text{m}^{-1}\ \text{s}])^{0.33} + 1.0\dfrac{U}{U_o^d} & U + U_o^d \ge 0. \end{cases} \tag{33}$$

On the upwind side,

$$f(U, U_o^u)_{\overline{w_s\theta'}^p} = \begin{cases} 1.0 - 0.1\dfrac{U}{U_o^{u,\theta}} & U - U_o^{u,\theta} < 0 \\ 0.9 + 2.0\dfrac{U}{U_o^{u,\theta}} & U + U_o^{u,\theta} \ge 0, \end{cases} \tag{34}$$

$$f(U, U_o^u)_{\overline{w_s q'}^p} = \begin{cases} 0.9 + 0.2\dfrac{U}{U_o^{u,q}} & U \ge U_o^{u,q}. \end{cases} \tag{35}$$

Here, we assume that $U_o^d = 0.5 + 7.9 \times 10^{-3}$ s^{-1} [m$^{0.5}$] $L^{0.5}$ (=2.5 m s^{-1} for a 64-km patch). The parameter $U_o^{u,q} = 0.5$ m s^{-1}, while $U_o^{u,\theta} = U_o^d$.

The dimensionless number, D^1, is the same as above:

$$D^1_{\overline{w_s\theta'}^p} = xe^{-0.50x}, \tag{36}$$

$$D^1_{\overline{w_s q'}^p} = xe^{-0.50x}. \tag{37}$$

We use the model output discussed in Part 1 to obtain the complete set of dimensionless numbers, including the fluxes. We used all of the simulations with moist processes turned off, and one with moist processes turned on (experiment 1w). We present the time dependence of the maximum values of each variable, in Figs. 10 and 11. When compared to Figs. 8 and 9, these figures demonstrate the ability of the parameterization to represent the sensitivity of the model results. We also calculated the mean and the absolute difference (after averaging the modeled fluxes every 30 min). For, $\overline{w_s\theta'}^p$, the mean was 0.37 K m s^{-1}, while the absolute difference was 0.13 K m s^{-1}. For $\overline{w_s q'}^p$, the mean was

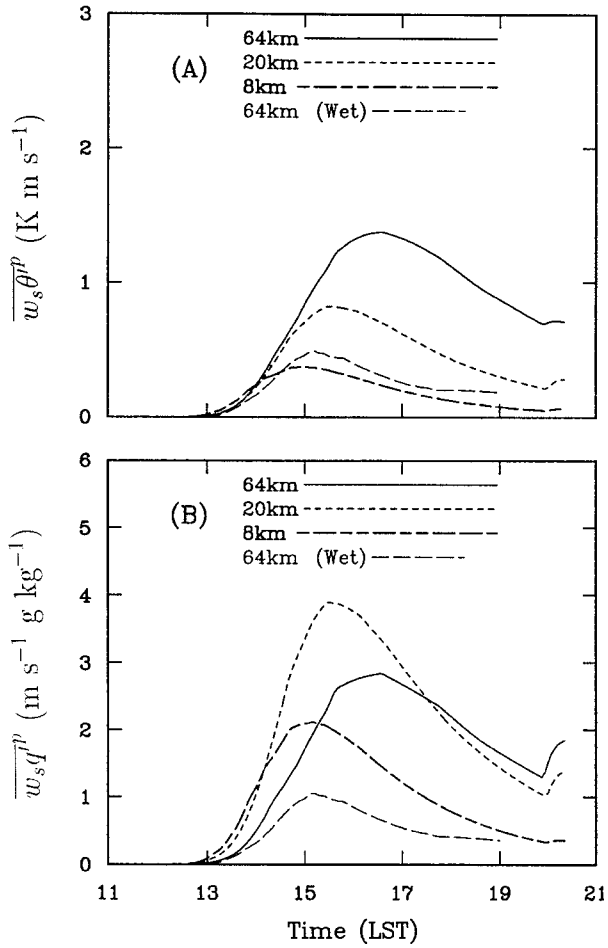

FIG. 10. Same as Fig. 8 but obtained with the parameterization.

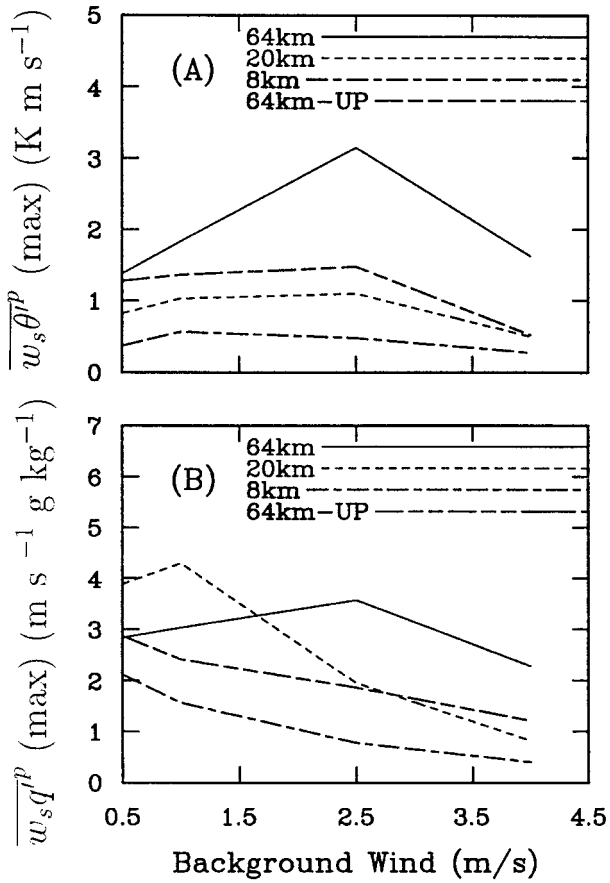

FIG. 11. Same as Fig. 9 but obtained with the parameterization.

0.70 m s^{-1} g kg^{-1}, while the absolute difference was 0.40 m s^{-1} g kg^{-1}. We noted that the absolute difference for the moisture flux was not small. This was mostly because the averaged data for this flux varied irregularly in time.

To differently and perhaps better compare the model results with the parameterization, we calculated the integral of the fluxes. The parameterized sensible heat fluxes were the same as the modeled fluxes, while the parameterized moisture fluxes were about 12% larger than the modeled fluxes. Small decreases in the intergral fluxes were obtained when the last 2 h of data were excluded from the integration. In summary, this parameterization captured the most important features of the model output: (i) the dependence upon patch size, (ii) background wind, (iii) stability, and (iv) specific humidity, including moist processes.

4. Summary and conclusions

A set of relatively high-resolution three-dimensional simulations were produced to investigate the triggering of moist convection over heterogeneous, west-to-east land surface domains. This moist convection was triggered by mesoscale circulations generated by the landscape heterogeneity. We used a Fourier transform to filter the data, and obtain a distribution of mesoscale and turbulent perturbations. These fluctuations were averaged over the area of a triggering parcel, occurring along sea-breeze-like fronts associated with the landscape-generated mesoscale circulations. We developed both zero-order and first-order closure to address the problem of triggering of moist convection by landscape patches.

To use the zero-order scheme, one need only obtain the parameters presented in Table 1. These are used to calculate various dimensionless numbers. These parameters can be obtained from the large-scale, hosting model, and from land surface models that retain soil moisture distribution within each grid of the hosting model, for example, models like TOPMODEL-based Land–Atmosphere-Transfer-Scheme (e.g., Peters-Lidard et al. 1997). In regard to the latter, a power spectrum of the land surface moisture distribution could be used as a guide to obtain patch sizes [see Fig. 3 of Lynn et al. (2001)]. Equation (12) can then be used to obtain the time dependence of the maximum in the mesocale triggering variables. We also provide empirical rela-

tionships for each triggering function that define how each varies with height.

Alternatively, we derived budget equations for θ_o and q_o, the vertical profiles of temperature and moisture, respectively, for parcels moving along sea-breeze-like fronts. These equations contain contributions from mesoscale and turbulent fluxes, as well terms such as $\overline{w_s\theta'^p}$ and $\overline{w_s q'^p}$ (which represent the vertical flux of the mesoscale temperature and moisture perturbation, respectively). We calculated the various terms in the budget equations and determined that only $\overline{w_s\theta'^p}$ and $\overline{w_s' q'^p}$ needed to be parameterized to close each respective equation. To do so implies first-order closure. The parameterization presented here used similarity theory to obtain these fluxes. The budget equations could be used to provide an alternative means of evaluating when and where convection occurs.

To use the first-order closure requires all the parameters in Table 1, the implementation of the set of budget equations, as well as Eq. (27). This is more complex than with zero-order closure, but has two possible advantages: (i) First order-closure has been found to better represent the evolution of the planetary boundary layer than zero-order closure (e.g., Stull 1989). Thus, the use of budget equations for a parcel's temperature and moisture profile will likely produce more realistic results than the zero-order scheme. (ii) The advantage of being better able to represent the effect of moist processes on the triggering variables. Changes in the vertical structure of the profiles of θ_o and q_o with the development of moist convection could have an important impact on the convective development that might occur after the initial triggering of either shallow or deep moist convection. Another possible advantage, (iii), is that the use of the budget equations precludes the need to estimate a parcel's turbulent fluctuations in temperature and moisture. These fluctuations, we found, were very sensitive to size of the parcel.

It might be interesting to note that the vertical structure of the grid-scale mesoscale fluxes are also insensitive to phase transitions. Therefore, the parameterizations developed by Lynn et al. (1995a) and Zeng and Pielke (1995) should also apply as given for both dry and moist regimes.

Acknowledgments. The first author was supported by a National Aeronautics and Space Administration Cooperative Agreement NCC 5-82. The second author is supported by the NASA Headquarters physical climate program, the NASA TRMM, and the interdisciplinary program of EOS. Each author thanks Drs. R. Adler and R. Kakar for their support, and two reviewers and Dr. D. Baker for their helpful and constructive suggestions. The views expressed herein are those of the authors and do not necessarily reflect the views of either agency.

REFERENCES

Avissar, R., and F. Chen, 1993: Development and analysis of prognostic equations for mesoscale kinetic energy and mesoscale (subgrid-scale) fluxes for large scale atmospheric models. *J. Atmos. Sci.,* **50,** 3751–3774.

Chen, F., and R. Avissar, 1994: Impact of land-surface moisture variability on local shallow convective cumulus and precipitation in large-scale models. *J. Appl. Meteor.,* **33,** 1382–1401.

Clark, C. A., and R. W. Arritt, 1995: Numerical simulations of the effect of soil moisture and vegetation cover on the development of deep convection. *J. Appl. Meteor.,* **34,** 2029–2045.

Cutrim, E., D. W. Martin, and R. Rabin, 1995: Enhancement of cumulus clouds over deforested lands in Amazonia. *Bull. Amer. Meteor. Soc.,* **76,** 1801–1805.

Dudhia, J., 1993: A nonhydrostatic version of the Penn State–NCAR Mesoscale Model: Validation tests and simulation of an Atlantic cyclone and cold front. *Mon. Wea. Rev.,* **121,** 1493–1513.

Frank, W. M., 1983: The cumulus parameterization problem. *Mon. Wea. Rev.,* **111,** 1859–1870.

Hong, S.-Y. and H.-L. Pan, 1998: Convective trigger function for a mass-flux cumulus parameterization scheme. *Mon. Wea. Rev.,* **126,** 2599–2620.

Hong, X., M. J. Leach, and S. Raman, 1995: A sensitivity study of convective cloud formation by vegetation forcing with different atmospheric conditions. *J. Appl. Meteor.,* **34,** 2008–2028.

Kain, J. S., and J. M. Fritsch, 1990: A one dimensional entraining/detraining plume model and its application to convective parameterization. *J. Atmos. Sci.,* **47,** 2784–2802.

Lynn, B. H., F. Abramopoulos, and R. Avissar, 1995a: Using similarity theory to parameterize the mesoscale fluxes generated by landscape discontinuities in GCMs. *J. Climate,* **8,** 932–951.

——, D. Rind, and R. Avissar, 1995b: The importance of mesoscale circulations generated by subgrid-scale landscape heterogeneities in general circulation models. *J. Climate,* **8,** 191–205.

——, W.-K. Tao, and P. J. Wetzel, 1998: A study of landscape generated deep moist convection. *Mon. Wea. Rev.,* **126,** 928–942.

——, ——, and F. Abramopoulos, 2001: A parameterization for the triggering of landscape-generated moist convection, Part I: Analysis of high-resolution-model results. *J. Atmos. Sci.,* **58,** 575–592.

Peters-Lidard, C. D., M. S. Zion, and E. F. Wood, 1997: A soil–vegetation–atmosphere transfer scheme for modeling spatially variable water and energy balance processes. *J. Geophys. Res.,* **102** (D4), 4303–4334.

Pielke, R. A., 1984: *Mesoscale Numerical Modelling.* Academic Press, 612 pp.

——, G. A. Dalu, J. S. Snook, T. J. Lee, and T. G. F. Kittel, 1991: Nonlinear influence of mesoscale land use on weather and climate. *J. Climate,* **4,** 1053–1069.

——, T. J. Lee, J. H. Copeland, J. L. Eastman, C. L. Ziegler, and C. A. Finley, 1997: Use of USGS-provided data to improve weather and climate simulations. *Ecol. Appl.,* **7,** 3–21.

Rabin, R. M., S. Stadler, P. J. Wetzel, D. J. Stensrud, and M. Gregory, 1990: Observed effects of landscape variability on convective clouds. *Bull. Amer. Meteor. Soc.,* **71,** 272–280.

Rogers, R. F., and J. M. Fritsch, 1996: A general framework for convective trigger functions. *Mon. Wea. Rev.,* **124,** 2438–2452.

Stauffer, D. R., R. C. Munoz, and N. L Seaman, 1999: In-cloud turbulence and explicit microphysics in the MM5. Preprints, *Ninth MM5 Users Workshop,* Boulder, CO, NCAR, 177–180.

Stull, R. B., 1988: *An Introduction to Boundary Layer Meteorology.* Kluwer, 666 pp.

Tao, W. K., and J. Simpson, 1993: Goddard Cumulus Ensemble Model. Part I: Model description. *TAO,* **4,** 35–72.

Wetzel, P. J., and A. Boone, 1995: A parameterization for Land–Atmosphere–Cloud Exchange (PLACE): Documentation and testing of a detailed process model of the partly cloudy boundary layer over heterogeneous land. *J. Climate,* **8,** 1810–1837.

Zeng, X., and R. A. Pielke, 1995: Landscape-induced atmospheric flow and its parameterization in large-scale numerical models. *J. Climate,* **8,** 1156–1177.